# Observation of Alfvén Wave Reflection in the Solar Chromosphere: Ponderomotive Force and First Ionization Potential Effect – Supplemental Material

Mariarita Murabito, Marco Stangalini, J. Martin Laming, Deborah Baker, Andy S. H. To, David M. Long, David H. Brooks, Shahin Jafarzadeh, David B. Jess, Gherardo Valori

## I. PHASE LAG ANALYSIS

Following [1], it is possible to define the cross-power spectrum, $\Gamma_{12}(\nu)$, of two input time series, $T1$ and $T2$, as,

$$\Gamma_{12}(\nu) = F(T1) * \overline{F(T2)} \ , \tag{1}$$

where $F$ denotes the application of the Fast Fourier Transform (FFT), while $\overline{F}$ indicates the complex conjugate of the resulting FFT. The resulting cross-power spectrum is a complex array, containing components linked to its co-spectrum, $d(\nu)$, and quadrature spectrum, $c(\nu)$ [2]. To calculate the phase lag between the two input signals as a function of frequency, we follow the work of Penn et al. [3],

$$\phi(\nu) = \arctan\left(\frac{\left\langle c(\nu)\right\rangle}{\left\langle d(\nu)\right\rangle}\right) \ . \tag{2}$$

Here, the phase angle spans the interval $-180^\circ \leq \phi(\nu) \leq +180^\circ$ and is simply the phase of the complex cross-spectrum [4].

## II. CA II FORMATION HEIGHT

To estimate the formation heights associated with the sampled wavelength positions, we compute line-depression contribution functions (CF) by means of the 1D version of the RH code [7]. As such, the radiative transfer and statistical equilibrium equations, in non-LTE conditions, are solved in a 1D model atmosphere, based on the Multi-level Accelerated Lambda Iteration (MALI) scheme of [8, 9]. Hence, an emergent-intensity Ca II 854.2 nm spectral line is first perturbed in a model atmosphere, from which the CFs are calculated. Consequently, the CFs, at each wavelength position, are convolved with the transmission profile of the IBIS Ca II 854.2 nm narrowband filter [10].

Figure 1 summarises the results. The upper-left panel illustrates the synthetic line (from the solar atlas) along with the DST/IBIS transmission profiles (dashed lines) and the convolved spectra (red solid lines) at the sampled (observed) wavelength positions. An average IBIS Ca II 854.2 nm spectral line (averaged over a small IBIS field of view) is shown on the upper-right panel, where all sampled wavelength positions are also marked. The six wavelength positions of interest for which the phase lags were calculated in the main text (see Figure 2) are additionally identified, for which the contribution functions are plotted on the lower-left panel. The widths of the CFs somewhat relate to the width of the transmission profile, thus, there is a relatively wide range of heights associated with each wavelength position. However, statistically speaking, they represent distinct mean heights of formation, summarised on the lower-right panel.

For consistency with the earlier modelling in the present work, we chose to carry out the CF computation in the FALC model atmosphere [11, 12] which was reconstructed to represent an averaged quiet-Sun. Although the FALC model may not best describe the active region under study, we found that the differences between FALC and, e.g., FALP (representing kG plage regions), are not large, with differences on the order of 20-170 km, on average, when computed at different wavelength positions. We emphasise that these initial estimates should still serve as a good height approximation for the purpose of the present study, even for comparing the phase lags from the Stokes $V$ signals (for which computation of response functions to the magnetic field, though challenging, would provide a more accurate estimation).

## III. ALFVÉN WAVE PROPAGATION MODELS

We model the Alfvén wave propagation by constructing loops, straightened out, with a chromosphere [11] added at each end. Loop parameters are chosen to give resonant frequencies of 3.04 mHz for Box A and 0.102 Hz for the BDs. For Box A we also consider the first and second harmonics at 5.55 and 8.28 mHz respectively. These are not quite two and three times the fundamental frequency because higher frequency waves propagate deeper into the chromosphere before reflecting back upwards again, i.e. higher frequency waves "see" a slightly longer loop. The chromospheric magnetic field is taken to be 1500 G, and the Alfvén wave transport is given by the numerical solution to the equations

$$\frac{\partial I_\pm}{\partial t} + (u \mp V_A)\frac{\partial I_\pm}{\partial z} = (u \pm V_A)\left(\frac{I_\pm}{4H_D} + \frac{I_\mp}{2H_A}\right), \tag{3}$$

where $I_\pm = \delta\mathbf{v} \pm \delta\mathbf{B}/\sqrt{4\pi\rho}$ are the Elsässer variables representing waves propagating in the $\mp$ z-directions, and $H_D$ and $H_A$ are the (signed) scale heights for density and Alfvén speed. In terms of $I_\pm$ the velocity and magnetic field perturbations are given by

$$\delta v = \frac{I_+ + I_-}{2}$$

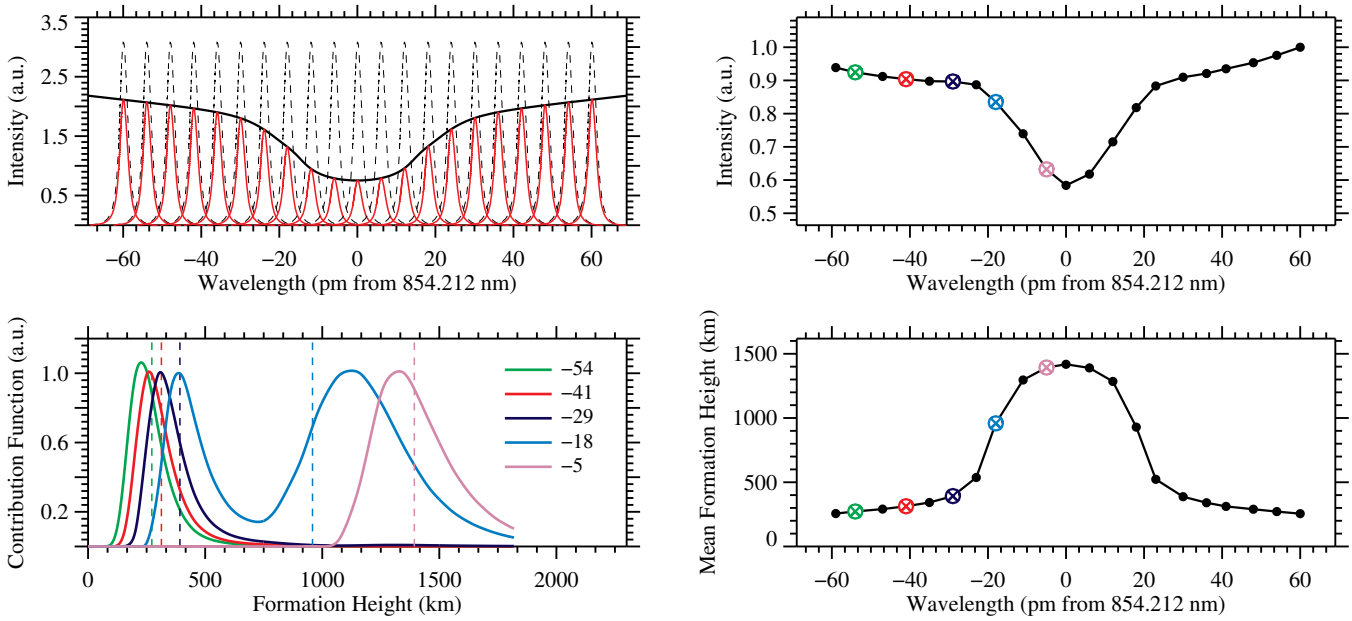


FIG. 1. Ca II 854.2 nm computed from the FALC model atmosphere. Top left: emergent-intensity spectra from the solar atlas. The dashed lines are the transmission profile of the DST/IBIS Ca II 854.2 nm filter, and the red solid curves are filter-transmitted intensity spectra, at the observed wavelength positions. Top right: observed Ca II 854.2 nm Stokes $I$ profile (averaged over a small IBIS field of view). All sampled wavelength positions, along with six points of interest, are marked. Bottom left: contribution functions, computed with the RH code, for the convolved transmitted intensities for the six points of interests (as also identified on both right panels; see the legend for the wavelength positions in pm from the Ca II line core). The first-moment height-of-formation averages are marked with the vertical dashed lines that are also summarised on the bottom-right panel (also for the other observed wavelength positions).

$$\frac{\delta B}{\sqrt{4\pi\rho}} = \frac{I_+ - I_-}{2}\,. \tag{4}$$

and the ponderomotive acceleration is

$$a = \frac{c^2}{2}\frac{\partial}{\partial z}\left(\frac{\delta E^2}{B^2}\right), \tag{5}$$

where $\delta E = \delta B V_A/c$ is the Alfvén wave electric field.

The elemental fractionation $f_k = \rho_k(z_u)/\rho_k(z_l)$ of element $k$ by the ponderomotive acceleration is given in the simplest case by the equation [13]

$$f_k = \exp\left\{\int_{z_l}^{z_u} \frac{2\xi_k a \nu_{kn}/\left[\xi_k\nu_{kn} + (1-\xi_k)\,\nu_{ki}\right]}{2k_\mathrm{B}T/m_k + v_{||,osc}^2 + 2u_k^2} dz\right\}. \tag{6}$$

Here, $\xi_k$ is the element ionization fraction and $\nu_{ki}$ and $\nu_{kn}$ are collision frequencies of ions and neutrals with the background gas. In the denominator, $k_\mathrm{B}T/m_k\,(=v_z^2)$ represents the square of the element thermal velocity along the $z$-direction, $u_k$ is the upward flow speed and $v_{||,osc}$ is a longitudinal oscillatory speed, corresponding to upward and downward propagating sound waves. These sound waves include those of photospheric origin propagating upwards, and those generated locally by the Alfvén wave driver, and are usually the main term in the denominator. Equation C4 is derived from the momentum equations for ions and neutrals in a background of protons and neutral hydrogen. These are integrated between upper and lower boundaries of the fractionation region, $z_u$ and $z_l$. Typically, $z_u$ is in the corona, where everything has become ionized, and $z_l$ is taken where the ratio of gas and magnetic pressures $\beta = 8\pi n k_\mathrm{B}T/B^2 = 1.2$. A rationale for this choice is given by [14], who argues that photospheric hydrodynamic turbulence is too strong to allow fractionation, while weaker MHD turbulence in the chromosphere has little effect.


[1] J.S. Bendat and A. G. Peirsol, BOOK REVIEW: Random Data Analysis and Measurement Procedures, Measurement Science and Technology 11, 1825 (2000). doi:10.1088/0957-0233/11/12/702

[2] D. B. Jess, S. Jafarzadeh, P. H. Keys et al., Living Reviews in Solar Physics 20, 1 (2023). doi:10.1007/s41116-022-00035-6

[3] M. J. Penn, T. Schad, and E. Cox, Astrophys. J.734, 47 (2011). doi:10.1088/0004-637X/734/1/47

[4] B. A. Vaughan and M. A. Nowak, Astrophys. J. Lett. 474, LL43 (1997). doi:10.1086/310430

[5] D. B. Jess, P. H. Keys, M. Stangalini et al., Philosophical

Transactions of the Royal Society of London Series A 379, 20200169 (2021). doi:10.1098/rsta.2020.0169
[6] D. Baker, D. H. Brooks, P. Démoulin et al., Astrophys. J.778, 69 (2013). doi:10.1088/0004-637X/778/1/69
[7] H. Uitenbroek, Astrophys. J.557, 389 (2001). doi:10.1086/321659
[8] G. B. Rybicki and D. G. Hummer, Astron. Astrophys. 245, 171 (1991).
[9] G. B. Rybicki and D. G. Hummer, Astron. Astrophys. 262, 209 (1992).
[10] K. Reardon and F. Cavallini, Mem. Soc. Astron. It. 74, 815 (2003).
[11] J. M. Fontenla, E. H. Avrett and R. Loeser, Astrophys. J.406, 319 (1993). doi:10.1086/172443
[12] J. M. Fontenla, W. Curdt, M. Haberreiter et al., Astrophys. J.707, 482 (2009). doi:10.1088/0004-637X/707/1/482
[13] J. M. Laming, Astrophys. J.844, 153 (2017). doi:10.3847/1538-4357/aa7cf1
[14] J. M. Laming, Astrophys. J.909, 17 (2021). doi:10.3847/1538-4357/abd9c3